

Leveraging chaos in the training of artificial neural networks

Pedro Jiménez-González, Miguel C. Soriano and Lucas Lacasa
*Institute for Cross-Disciplinary Physics and Complex Systems (IFISC, CSIC-UIB),
Campus UIB, 07122 Palma de Mallorca, Spain*

Traditional algorithms to optimize artificial neural networks when confronted with a supervised learning task are usually exploitation-type relaxational dynamics such as gradient descent (GD). Here, we explore the dynamics of the neural network trajectory along training for unconventionally large learning rates. We show that for a region of values of the learning rate, the GD optimization shifts away from purely exploitation-like algorithm into a regime of exploration-exploitation balance, as the neural network is still capable of learning but the trajectory shows sensitive dependence on initial conditions –as characterized by positive network maximum Lyapunov exponent–. Interestingly, the characteristic training time required to reach an acceptable accuracy in the test set reaches a minimum precisely in such learning rate region, further suggesting that one can accelerate the training of artificial neural networks by locating at the onset of chaos. Our results –initially illustrated for the MNIST classification task– qualitatively hold for a range of supervised learning tasks, learning architectures and other hyperparameters, and showcase the emergent, constructive role of transient chaotic dynamics in the training of artificial neural networks.

The multilayer perceptron (MLP) is an archetypical method in supervised machine learning [1, 2], used to infer (regress or classify) complex input-output representations $x \rightarrow y$, where $x \in \mathbb{R}^m$ and y is usually another vector for regression tasks or an element from a discrete set in classification tasks. Accordingly, an MLP is mathematically an overparametrized nonlinear function $\mathcal{F}(x; \Omega)$, where $\Omega = \{\omega_k\}$ is the set of trainable parameters. Often represented as an (artificial neural) network [1, 2], the MLP is visualized as a mathematical graph composed of various stacked layers of interconnected nodes, where the first layer represents the input vector $x \in \mathbb{R}^m$. The edges connecting nodes in adjacent layers represent (parametric) affine transformations of the vector elements of one layer to the next one (the coefficients of such transformations, usually called the edge weights, belong to the parameter set Ω), and the nodes integrate the incident linear compositions in the edges nonlinearly via what is called an activation function. The information thus flows from the input layer x onwards until reaching the final, output layer whose nodes represent the elements of the output $y = \mathcal{F}(x; \Omega)$. Optimizing the set of parameters Ω so that the mismatch between $\mathcal{F}(x; \Omega)$ and y –the so-called loss function $\mathcal{L}(x; \Omega)$ – is minimized is called the *training* process. In practice, training the MLP is usually done iteratively, being gradient descent (GD) in parameter space the gold standard, where

$$\omega_k(t+1) = \omega_k(t) - \eta \partial_{\omega_k} \mathcal{L}(x; \Omega(t)), \quad \forall \omega_k \in \Omega \quad (1)$$

where η is the so-called learning rate and $\partial_x := \partial/\partial x$.

Observe that, along training, the MLP is effectively performing a trajectory in the (graph) space spanned by the set of parameters Ω . We contend that reinterpreting the training process as a (high-dimensional, latent) graph dynamics [3] allows to inquire the inner workings of learning algorithms following physics-inspired and complexity-based epistemics [4–6]. Instead of tracking the scalar

projection of the full dynamics given by the time evolution of the loss function $\mathcal{L}(x; \Omega(t))$, let us consider the actual network trajectory [7]. We argue that this change of focus –which amounts to tracking full graph trajectories of the form $(\Omega(0), \Omega(1), \Omega(2) \dots)$, where the set $\Omega(t) = \{\omega_1(t), \dots, \omega_m(t)\}$ incorporates the updated values of the so-called weights and biases of the neural architecture at training epoch t – can provide valuable insights if at the same time we leverage principles and tools from network science [8–13] and dynamical systems [14, 15].

Along training, a priori one assumes that a typical network trajectory is non-ergodic: there is an arrow of time induced by the relaxational nature of Eq. 1 which is inherited in graph space. This intuition is indeed intimately related to the convergence properties of the GD scheme to local minima of $\mathcal{L}(x; \Omega)$. Accordingly, GD [16] is often seen as an *exploitation* search algorithm, that iteratively performs small improvements of an initial solution, so that some fitness function (here the loss function \mathcal{L}) is gradually (e.g. monotonically) decreased. Now, GD convergence is not always fulfilled, specially for large enough learning rates, when GD can display more exotic behavior [17]. At the same time, convergence to local minima is an asymptotic behavior, and interesting dynamics often emerge in transient times [18]. Altogether, it is interesting to consider whether, led by qualitative dynamical changes in the behavior of GD-type maps, not just the loss function but the whole MLP network trajectories *transition* from following a pure exploitation strategy to other search strategies –such as *exploration* [19]– when the learning rate is large enough. Note that a similar balance of strategies [20] is known to yield optimal searching behaviors in animal foraging [21–27], transport [28] and a range of decision-making contexts [29, 30], and is an explicit cornerstone of the Reinforcement Learning paradigm [31].

Our contention in this work is that, indeed, such transition takes place, and the emergence of exploration-like dynamics is induced by the onset of sensitive dependence

on initial conditions –the hallmark of chaotic dynamics– in the dynamics of Eq. 1. Let us clarify at this point that in this work we are not considering intrinsically dynamic neural networks whose neurons show chaotic behavior [32–37], instead we are considering the training (optimization) dynamics in a neural network whose output is not dynamic. Moreover, we argue that (i) for an often unexplored region of large-but-not-too-large values of η , the map is optimally interpolating exploitation and exploration search strategies, and (ii) that the average training time required to reach a performance on the test set $\text{Test} = \{x_i, y_i\}_{i=1}^{N_{\text{test}}}$ is minimized in such *sweet spot*. Interestingly, this coincides with a similar type of optimality emerging when the loss function’s Hessian asymptotically evolves over training towards its so-called edge-of-stability, i.e. when its largest eigenvalue approaches $2/\eta$ [38]. In a nutshell, we argue that the transition to an exploitation-exploration balance is achieved by leveraging the onset of transient chaotic mixing [18], and at such transition the system efficiently minimizes training time, resulting in a possible demonstration of Langton’s hypothesis [39].

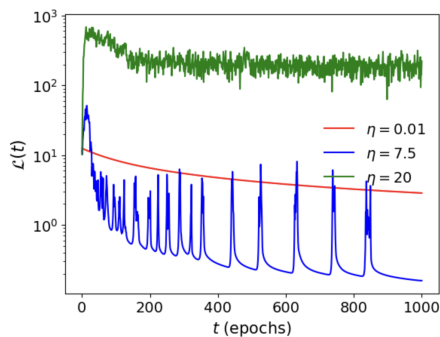


Figure 1: Training loss trajectory of a neural network on the MNIST dataset for three different learning rates: $\eta = 0.01$, $\eta = 7.5$ and $\eta = 20$.

To actually demonstrate our hypothesis, we initially consider a vanilla classification task: MNIST image classification [40]. For parsimony, we initially choose a shallow MLP (one hidden layer with 64 neurons) and a tanh activation function (the results for other supervised learning tasks, activation functions and deeper architectures are discussed in the Supplementary Figures S3-S7). After train/test split, this MLP is trained on a set $\text{Train} = \{(x_i, y_i)\}_{i=1}^N$ of $N = 6 \cdot 10^4$ labelled handwritten images (y_i is the label of the i -th image), and we use a cross-entropy loss function

$$\mathcal{L}(x; \Omega) = -\frac{1}{N} \sum_{i=1}^N y_i \log \mathcal{F}(x_i; \Omega). \quad (2)$$

Training takes place by using Eq. 1. For the sake of simplicity, no regularization is initially added to the loss function (results with L_2 weight regularization are discussed in Supplementary Fig. S6). Additionally, we use

traditional GD schemes (no mini-batch or SGD) and discard dropout to remove any source of stochasticity to the network dynamics [17]. Finally, to assess the performance for different learning rates, a constant learning rate η is fixed throughout training.

Fig. 1 plots the time evolution of the (training) loss function $\mathcal{L}(x; \Omega(t)) \equiv \mathcal{L}(t)$ for three different learning rates η . Interestingly, such loss is only monotonically decreasing for the standard range of small values of the learning rate. For larger values of η other dynamical behaviors are found: converging loss functions with non-monotonic, irregular transients and other dynamical attractors for extremely large η , where the MLP does not seem to make any useful learning.

To better characterize what particular change in dynamical behaviors in the network evolution is inducing these projections in the loss function, we now resort to recently-introduced graph-theoretical extensions of the Maximum Lyapunov Exponent [41], designed to estimate sensitivity to initial conditions in network trajectories. The procedure consists in three steps: (i) for a fixed learning rate, we define a set of q different network initializations $\mathcal{S} = \{\Omega(0)\}$. (ii) Around each concrete network initialization $\Omega(0)$, we build an ϵ -ball formed by a set of M small network ‘perturbations’ of $\mathcal{B} = \{\Omega(0)^{(j)}\}_{j=1}^M$. To do that, we perturb each trainable parameter $w_k \in \Omega$ with uniform noise $w'_k = w_k + \xi$, $\xi \sim \text{UNIFORM}(-\epsilon, \epsilon)$. Defining the distance between two network initializations Ω, Ω' as the L_1 norm $d(\Omega, \Omega') = \sum_{\omega_k \in \Omega} |\omega_k - \omega'_k|$, it follows that each perturbed network $\Omega(0)^{(j)}$ is at most at distance $\text{CARD}(\Omega) \cdot \epsilon$ from $\Omega(0)$. (iii) Then, following [41] we measure the expansion rate of closeby network trajectories by adequately averaging the divergence of the M elements inside each ϵ -ball throughout the action of the training dynamics in Eq. 1:

$$\Lambda_{\Omega(0)} = \frac{1}{\tau} \ln \frac{M^{-1} \sum_{j=1}^M d_j(\tau)}{M^{-1} \sum_{j=1}^M d_j(0)}, \quad (3)$$

where $d_j(\tau) \equiv d(\Omega(\tau), \Omega(\tau)^{(j)})$. $\Lambda_{\Omega(0)}$ is indeed the network version of a finite, local Lyapunov exponent [41], where τ is the characteristic time required for the elements inside the ϵ -ball centered at $\Omega(0)$ to diverge to distances of the order of the phase space diameter. For an illustration, in Fig. 2 we depict the distance $d(t)$ between $M = 5$ network initializations close to an initial condition $\Omega(0)$ ($\epsilon = 10^{-8}$), for a large learning rate $\eta = 10$. We observe a clear exponential phase up to $\tau \approx 30$ epochs, the slope denoting the finite local network Lyapunov exponent $\Lambda_{\Omega(0)}$.

The network’s Maximum Lyapunov exponent averages the local exponents over different network initializations $\lambda_{\text{nMLE}} = \langle \Lambda_{\Omega(0)} \rangle_{\Omega(0) \in \mathcal{S}}$. For illustration, this is displayed for $\text{CARD}(\mathcal{S}) = 50$ different initial conditions in Fig. 3. The inset of that panel depicts the histogram of local exponents, whose average gives $\lambda_{\text{nMLE}} \approx 0.68$, i.e. the system shows sensitivity to initial conditions.

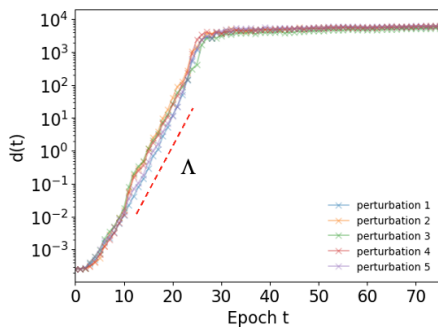


Figure 2: Semi-log plot of the evolution (along training) of the network distance $d(t)$ for pairs of network trajectories with closely initialization $\Omega(0)$, as a function of the number of epochs t , for a shallow MLP with $\tanh()$ activation function trained on MNIST with a large learning rate. $d(t)$ displays a stylized exponential expansion followed by saturation. The slope of the exponential phase corresponds to the local network Lyapunov exponent Λ and is indicative of chaotic mixing.

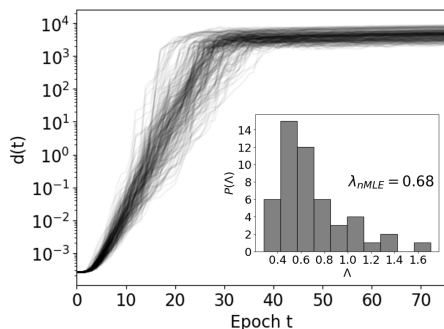


Figure 3: Same as Fig 2, but for many different ϵ -balls centered at different initial conditions Ω . Each initial condition leads in principle to a different local network Lyapunov exponent $\Lambda(\Omega)$. In the inset, we display the histogram of local network Lyapunov exponents. The average of this distribution is the estimation of the network MLE $\lambda_{nMLE} \approx 0.68$.

λ_{nMLE} can thus be seen as an order parameter distinguishing two phases: a phase where the search strategy induced by the GD map Eq. 1 is an exploitation one and $\lambda_{nMLE} \leq 0$, and a phase where the search strategy is of an exploration type with sensitive dependence on initial conditions, and $\lambda_{nMLE} > 0$. The transition between both phases interpolates both search strategies. As a complementary metric that will later assists us in our empirical analysis of the network training dynamics, we also define ρ as the percentage of MLP initializations of the set \mathcal{S} for which the ϵ -ball expansion can be well approximated by an exponential function with high statistical significance ($R^2 > 0.9$, $\Lambda > 0.05$), i.e this is the percentage of local network Lyapunov exponents which are positive.

In Fig. 4 we report λ_{nMLE} as a function of the gradi-

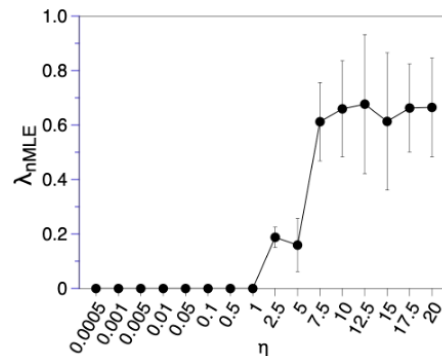


Figure 4: Estimation of the network Maximum Lyapunov Exponent λ_{nMLE} for MLP trajectories as a function of the learning rate η . Error bars denote \pm one standard deviation of the population of finite local network Lyapunov exponents $\{\Lambda(\Omega)\}$. The onset of sensitivity to initial conditions $\lambda_{nMLE} > 0$ marks the change from a purely exploitation-type optimization to an exploration/exploitation type.

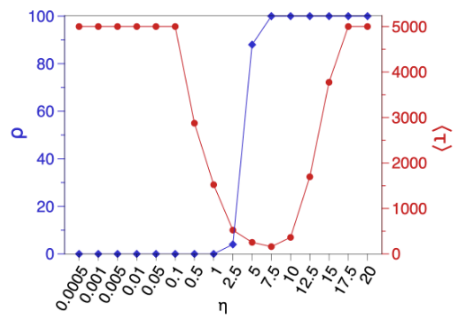


Figure 5: Blue diamonds depict ρ , the percentage of MLP initializations Ω leading to training trajectories with positive local Lyapunov exponent $\Lambda(\Omega) > 0$ as a function of the learning rate η . In the same figure, we also plot (red dots) the average training time $\langle \tau \rangle$ (in number of Gradient Descent epochs) needed to reach an accuracy of 90% or larger in the test set. Training is found to be maximally efficient close to the onset of fully-developed sensitivity to initial conditions ($\Lambda(\Omega) > 0 \forall \Omega$).

ent descent's learning rate η . Results indicate that there is a clear transition between exploitation to exploration search, where the exploitation-exploration interpolation hovers in the range $\eta \in [1, 10]$. Fig 5 displays ρ as a function of the learning rate. This metric confirms a transition between a phase where no initial conditions display exponential expansion, to a phase where virtually all regions of the phase space display chaotic transients. Finally, to assess the MLP's learning and training efficiency in the context of the abovementioned phenomenology, Fig. 5 also depicts the average number of epochs $\langle \tau \rangle$ needed for the MLP to reach an average classification accuracy of at least 0.9 in the test set (this is averaged over all different MLP initializations in \mathcal{S}), as a function of the learning rate η . We find that $\langle \tau \rangle$ displays a

non-monotonic shape, and indeed reaches a minimum in the exploitation-exploration interpolation region, at the learning rate $\eta \approx 7.5$, precisely marking the onset of fully-developed sensitivity to initial conditions $\rho \approx 100\%$.

As advanced, this type of optimality in the training dynamics has been recently observed when the largest eigenvalue σ_{\max} of the loss function’s Hessian asymptotically converges to $2/\eta$, the so-called edge of stability [38]. In Supplementary Fig. S8, we show how the time series of $\sigma_{\max}(t)$ over training indeed approaches $2/\eta$ when the learning rate hovers around the values for which $\langle \tau \rangle$ is minimized, and suggests that asymptotically self-organizing around the Hessian’s edge-of-stability is pre-cursed by a chaotic transient.

Our results are reasonably robust against changes in the classification task (see Supplementary Fig. S3 and S7 for further results on the Iris and CIFAR10 classification respectively), the type of activation function (see Supplementary Fig. S4 for further results with sigmoid and ReLU functions), the depth of the MLP (see Supplementary Fig. S5 for a comparison of shallow vs deep network), or the inclusion of weight regularization (see Supplementary Fig. S6), and overall highlight the relevance of leveraging chaotic mixing in the training of neural networks. In summary, we have found that, as the learning rate increases, the training dynamics transition from a regular, purely exploitation-type dynamics to a chaotic, purely exploration-type dynamics. The transition between both types is rather sharp and occurs in a region that trades-off exploitation and exploration by the onset of a mechanism of chaotic transient –emerging in the first few dozen epochs of the training dynamics–. This mechanism underpins an efficient search of graph space, eventually leading to faster learning. Evidence suggests that such early-stage, chaotic transient is pre-cursing at a later Hessian trajectories to eventually converge towards their edge of stability.

From a conceptual point of view, our findings suggest a demonstration of Langton’s edge of chaos hypothesis [39]. From an application side, we argue that this phenomenology could be leveraged to automatically boost the training efficiency of MLPs. As a matter of fact, while a priori the optimeal learning rate might depend on the specific task and architecture, results suggest that the existence of such optimal learning rate is universally valid. Accordingly, and since $\langle \tau \rangle$ is substantially reduced at such learning rate, one could e.g. use the bisection method to iteratively refine a learning rate range $[\eta_{\min}, \eta_{\max}]$ (such that in each step one runs the dynamics for a few dozen epochs and verify that $\rho(\eta_{\min}) \approx 0$ and $\rho(\eta_{\max}) \approx 100$) as a pre-processing before actually training the system.

Acknowledgments – The authors thank K. Danovski for input in preliminary stages of this project. PJ acknowledges funding from Maria de Maeztu (MdM) Seal of Excellence (CEX2021-001164-M) via the FPI programme (grant PRE2022-104148), funded by the MICIU/AEI/10.13039/501100011033. MCS and LL

acknowledge partial support from projects MISLAND (PID2020-114324GB-C22), MdM (CEX2021-001164-M) funded by the MICIU/AEI/10.13039/501100011033 and from the European Commission Chips Joint Undertaking project No. 101194363 (NEHIL).

Code availability – The code used to run the simulations will be available after publication at <https://github.com/pedrojg8>.

Supplementary Material

In this Supplementary Material we complement the results depicted in the main part of the paper by additionally testing (i) two additional datasets (Iris and CIFAR-10), (ii) two types of architectures (shallow vs deep MLP), (iii) three types of nonlinear activation function (sigmoid, ReLU and tanh), (iv) no regularization vs an L_2 type of network weight regularization. Results overall are in good agreement with the ones shown in the main text and support the robustness of the phenomenology.

I. TASK DATASETS: IRIS, MNIST AND CIFAR-10

For better interpretability of the training network dynamics, we use three vanilla datasets of increasing complexity for supervised classification: (i) IRIS [42], (ii) MNIST [43], and (iii) CIFAR-10 [44].

The **Iris dataset** [42] deals with classifying flower species. The dataset contains 150 samples, each characterized by 4 features (sepal length/width and petal length/width) and assigned to one of three species of *Iris* flowers. The dataset was divided into 120 samples for training and 30 samples for testing performance.

The **MNIST dataset** [43] is a well-known reference for image classification, especially in handwritten digit recognition. This dataset consists of 70,000 gray-scale images of digits (0 to 9), each normalized to a resolution of 28×28 pixels. It is divided into a training set of 60,000 images and a test set of 10,000 images, with all ten classes uniformly represented.

The use of IRIS and MNIST allows us to study how the network architecture and activation functions behave in different classification tasks. IRIS facilitates analysis in a low-dimensional space, while MNIST tests the network's ability to scale to more demanding learning tasks.

Finally, **CIFAR-10** [44] is a widely used benchmark for evaluating image classification models on natural images. It consists of 60,000 colour images of 32×32 pixels, extracted from 10 different classes: airplanes, automobiles, birds, cats, deer, dogs, frogs, horses, ships, and trucks, with 6,000 images per class. The dataset is divided into 50,000 images for training and 10,000 for testing. Each image is represented as a 3-channel RGB matrix, which makes this task considerably more complex than the greyscale digit classification task of MNIST.

II. ADDITIONAL RESULTS FOR DIFFERENT ARCHITECTURES, ACTIVATION FUNCTIONS AND REGULARIZATION TERMS

Architecture – We initially used a shallow (three-layer) MLP consisting of an input layer, a hidden layer and an output layer, forming a simple feedforward topology as illustrated in Figure S1. The input layer has n_I neurons, matching the dimensionality of the input data and serves as the entry point to the network. It is followed by a single hidden layer with n_H neurons, which introduces non-linearity through an activation function. The output layer, with n_O neurons, produces the final predictions and typically corresponds to the number of target classes or output variables. Each neuron in one layer is fully connected to all neurons in the next layer, forming a directed, layered architecture with no feedback or recurrence.

For the IRIS classification task, the network has $n_I = 4$, $n_H = 10$ and $n_O = 3$, giving a total of 83 trainable parameters. In the MNIST digit recognition task, the configuration is $n_I = 784$, $n_H = 64$ and $n_O = 10$, resulting in 50,890 trainable parameters. For the CIFAR-10 task, the network uses $n_I = 3072$, $n_H = 256$ and $n_O = 10$, giving a total of 789,258 trainable parameters.

To assess the universality of the results, we also investigate a deep architecture where we add an additional hidden layer. In order to allow for fair comparison, the total number of hidden neurons is kept fixed. This is performed on the MNIST task using the tanh activation function for both hidden layers. Specifically, the original single hidden layer with $n_H = 64$ is replaced by two hidden layers with $n_{H_1} = 32$ and $n_{H_2} = 32$ neurons, respectively. As a result, the total number of trainable parameters is reduced from 50,890 to 26,506.

Activation function – These are responsible for introducing non-linearity into the model, allowing the network to learn complex mappings between inputs and outputs [1]. Commonly used activation functions include the sigmoid, defined as $\sigma(x) = \frac{1}{1+e^{-x}}$, which maps inputs to the interval $[0,1]$; the hyperbolic tangent (tanh), given by $\tanh(x) = \frac{e^x - e^{-x}}{e^x + e^{-x}}$, which maps inputs to the range $[-1,1]$; and the Rectified Linear Unit (ReLU), defined as $\text{ReLU}(x) = \max(0, x)$, which outputs zero for negative inputs and retains the input value for positive ones. Figure S2 shows an illustration of the three activation functions described above. These three functions are included as representative cases due to

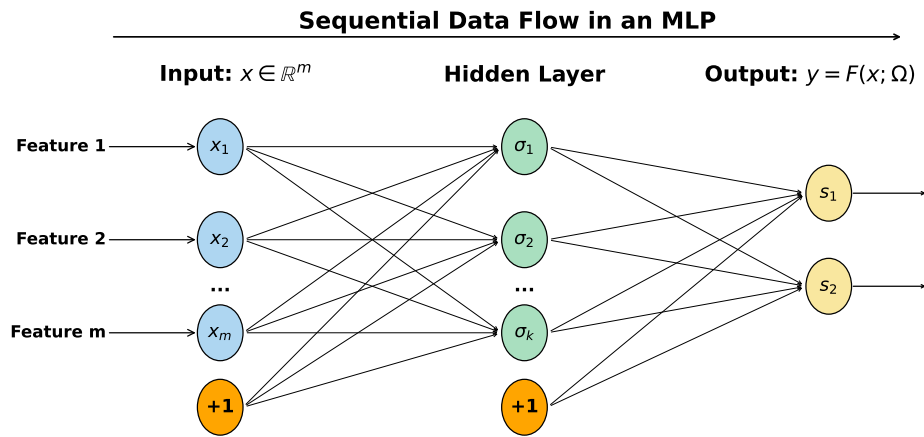


Figure S1: MLP topology.

their frequent use and different activation behaviours. Whereas results in the main part of the paper focus solely on the $\tanh(\cdot)$ activation function, here we also explore the sigmoid and ReLU.

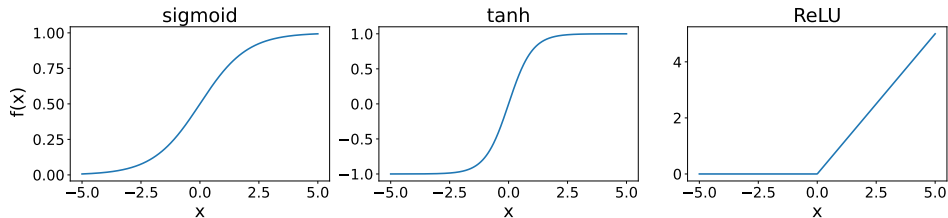


Figure S2: Illustration of the sigmoid, tanh, and ReLU activation functions.

Regularization – Finally, note that in the main text the loss function only included a cross-entropy term. Here we also assess the effect of introducing a standard L_2 weight regularization. The regularized loss function is given by:

$$\mathcal{L}_\lambda = \mathcal{L} + \frac{\lambda}{2} \|\mathcal{W}\|^2,$$

where \mathcal{L} denotes the original loss function, λ is the regularization strength (a hyperparameter of the network), and $\|\mathcal{W}\|^2$ represents the squared Frobenius norm of the weight matrices, that is, the sum of the squares of all trainable weight values in the network. For this experiment, we maintain the original network configuration (MNIST task with the tanh activation function and just one hidden layer).

III. ONSET OF SENSITIVITY TO INITIAL CONDITIONS AND TRAINING EFFICIENCY: SUPPLEMENTARY RESULTS

Below we present the results of the key metrics (network Maximum Lyapunov Exponent λ_{MLE} , percentage of positive finite network Lyapunov exponents ρ , and average training time $\langle \tau \rangle$) for the additional set of configurations and tasks (IRIS vs MNIST vs CIFAR-10, different activation functions, shallow vs deep architecture, effect of regularization). These results represent supporting evidence of the robustness of the phenomenology described in the main paper.

We start with the IRIS task and present the results in Figure S3, following the same methodology as in the main part of the paper. The results obtained using the IRIS dataset illustrate the behavior of the training network dynamics in a low-dimensional case. Due to its small size and low computational cost, IRIS provides an accessible testbed to validate the methodology before scaling it to more complex datasets. Results are qualitatively similar to the ones found in the main part of the paper.

IRIS TASK

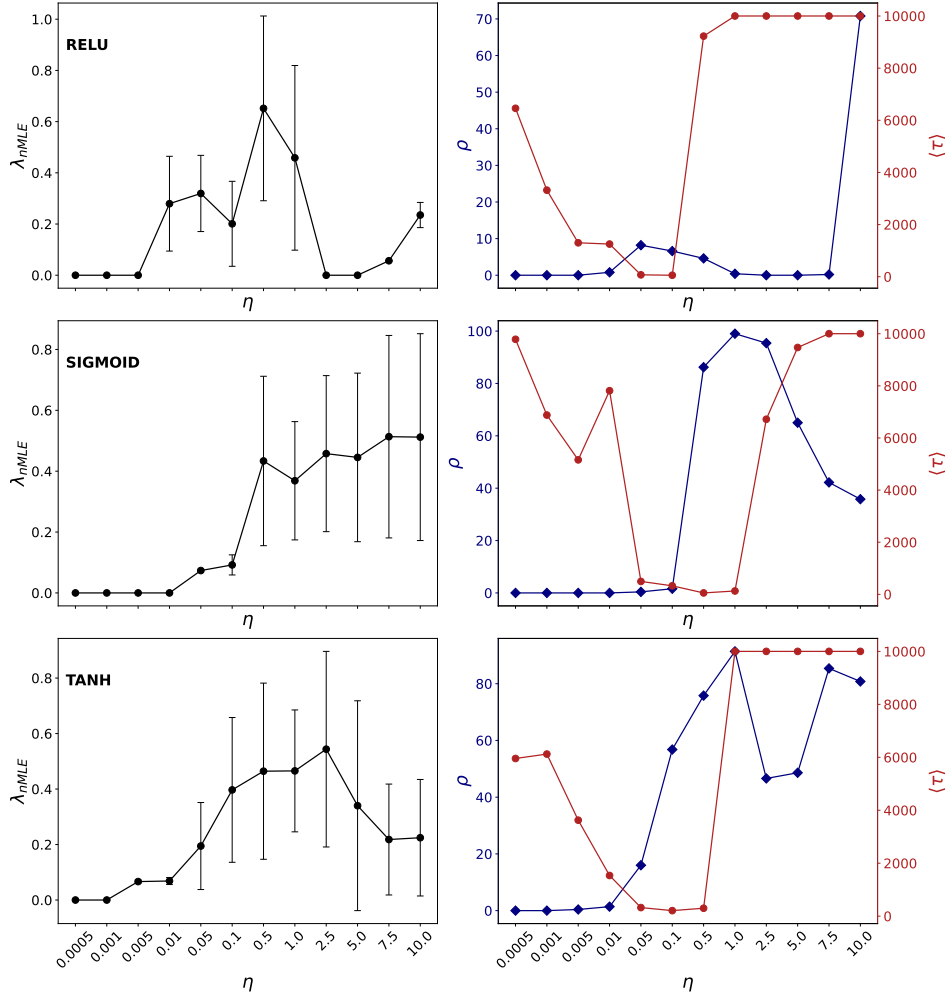


Figure S3: Lyapunov exponent (left column), percentage of valid exponents (ρ) and mean convergence time ($\langle\tau\rangle$) as functions of the learning rate (η) for each activation function. Results for the IRIS task.

In Figure S4 we come back to the MNIST task and present the results for different activation functions, highlighting the robustness of the patterns observed across different datasets and hyperparameters. For the sigmoid activation function, it should be noted that the minimum in $\langle\tau\rangle$ extends over a wide range of learning rates, forming a relatively flat region. To again observe the rise in the training time, you have to reach a learning rate value of $\eta = 30$.

The experiments with a deep architecture are presented in Figure S5, showing qualitatively similar phenomenology than the one found for the shallow architecture. In this case, the minimum number of epochs needed to reach the target accuracy is increased by a factor of 20 compared to the shallow configuration. Nevertheless, the phenomenon persists: there is still a clear minimum corresponding to the region of η where λ_{nMLE} starts to take positive values.

To conclude with the MNIST task, we present the results of the simulations with the inclusion of L_2 weight regularization in Figure S6. The regularization strength λ was set to 10^{-3} and 10^{-5} , chosen as representative values commonly used in practice to explore the influence of soft and weak regularisation effects. We also see that a suitable region appears if we look at the range of learning rate values that simultaneously minimise the training time of the network and exhibit chaotic dynamics.

Finally we present the results obtained for the CIFAR-10 task in Figure S7. Although the prediction task is not successfully solved, since it is not the main focus of our study, we include this case to demonstrate that the observed phenomenon persists. Networks with this type of topology (MLP) typically do not achieve accuracies higher than 50% on CIFAR-10. Achieving accuracies of approximately 70% usually requires more sophisticated MLP architectures,

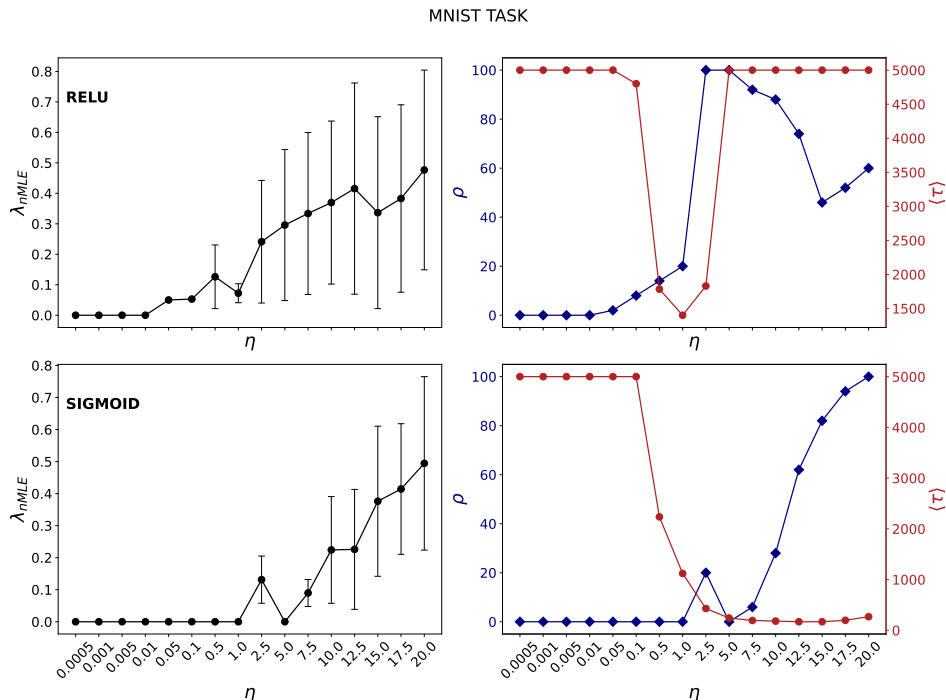


Figure S4: Lyapunov exponent (left column), percentage of valid exponents (ρ) and mean convergence time ($\langle \tau \rangle$) as functions of the learning rate (η) for the remaining activation functions. Results for the MNIST task.

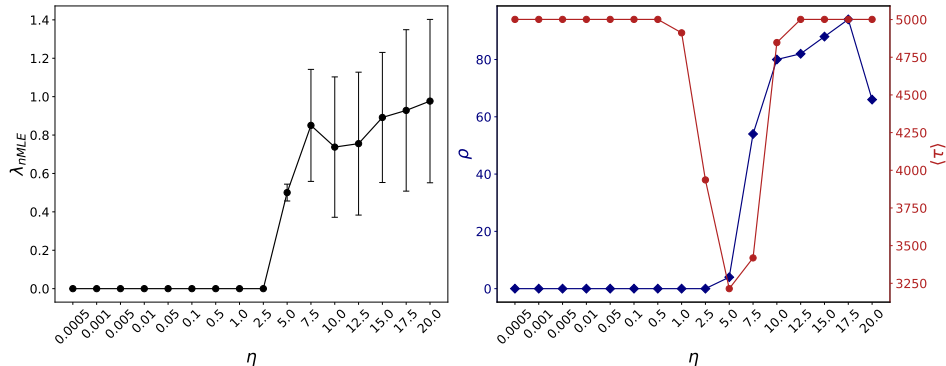


Figure S5: Lyapunov exponent (left column), percentage of valid exponents (ρ) and mean convergence time ($\langle \tau \rangle$) as functions of the learning rate (η). Results for the MNIST task with an extra hidden layer in the architecture and tanh as the activation function.

such as including the use of linear bottleneck layers [45]. For this reason, we lower the accuracy threshold to 30% and observe that the same characteristic behaviour is maintained.

EVOLUTION OF SHARPNESS

Following the approach in [38], we measure the evolution of sharpness during training, defined as the maximum eigenvalue of the Hessian of the training loss with respect to the model parameters. This measure characterises the local curvature of the loss surface and provides insight into the dynamics of the optimisation process. The sharpness is tracked across epochs for the model trained with the MNIST dataset and tanh as activation function.

We use power iteration to approximate the top eigenvalue of the Hessian. This method is computationally efficient and does not require explicit computation and storage of the full Hessian matrix, so it is feasible to apply it during training. We track the evolution of the sharpness over training by measuring the top eigenvalue of the Hessian matrix

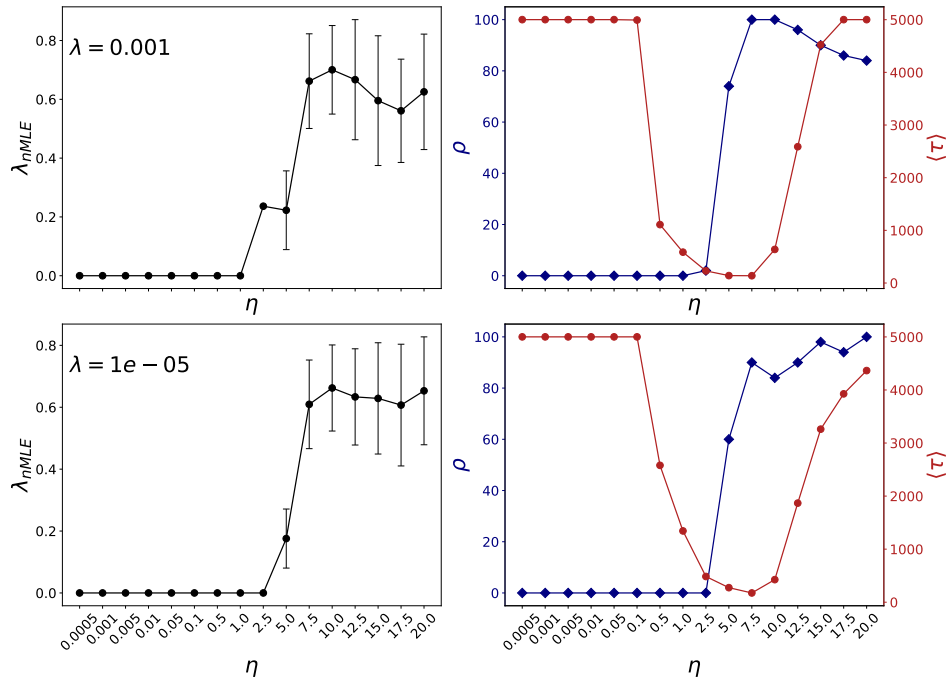


Figure S6: Lyapunov exponent (left column), percentage of valid exponents (ρ) and mean convergence time ($\langle \tau \rangle$) as functions of the learning rate (η). Results for the MNIST task with a single hidden layer and tanh activation function, now including L_2 -regularization.

of the loss function, as shown in Figure S8. For learning rates that minimize $\langle \tau \rangle$, we find that, in line with theoretical considerations [38], sharpness remains bounded once the training has stabilised and closely matches the theoretical limit of $2/\eta$, as indicated by the red dashed line. The results shown correspond to learning rates $\eta = 7.5$ and $\eta = 10$.

CIFAR-10 TASK

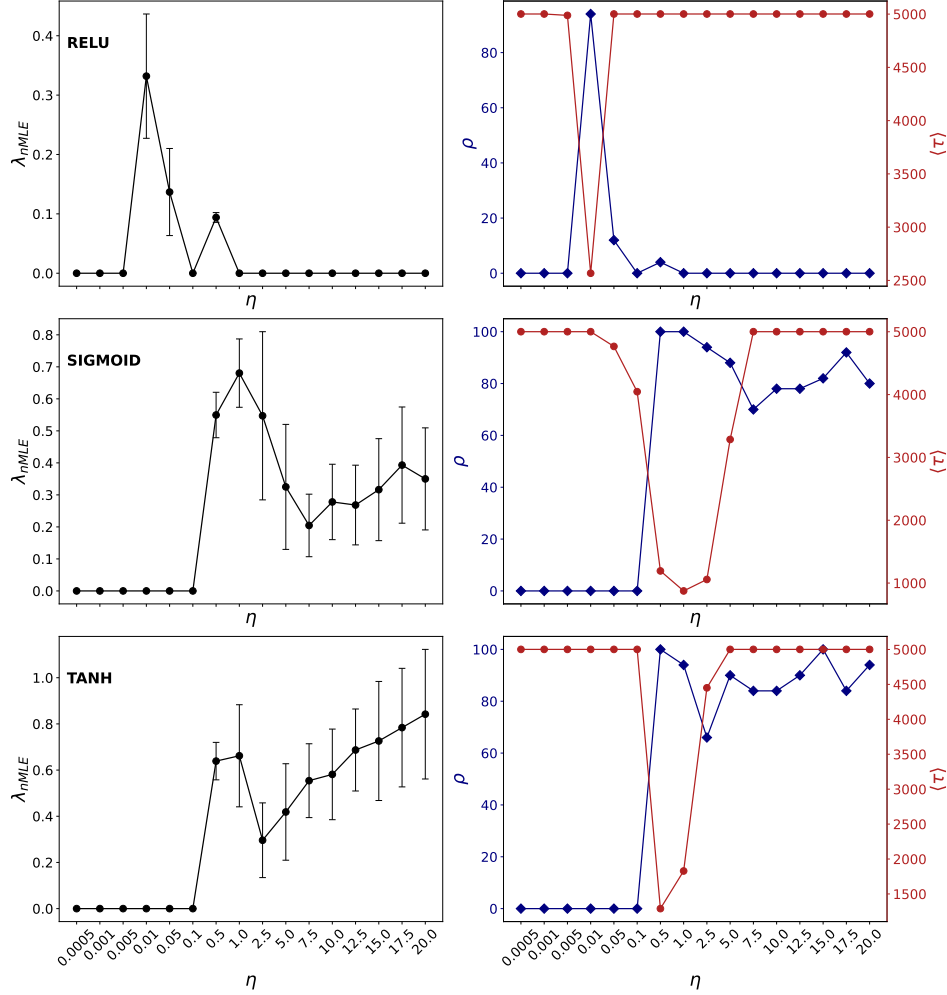


Figure S7: Lyapunov exponent (left column), percentage of valid exponents (ρ) and mean convergence time ($\langle \tau \rangle$) as functions of the learning rate (η) for each activation function. Results for the CIFAR-10 task with a target accuracy of 30%.

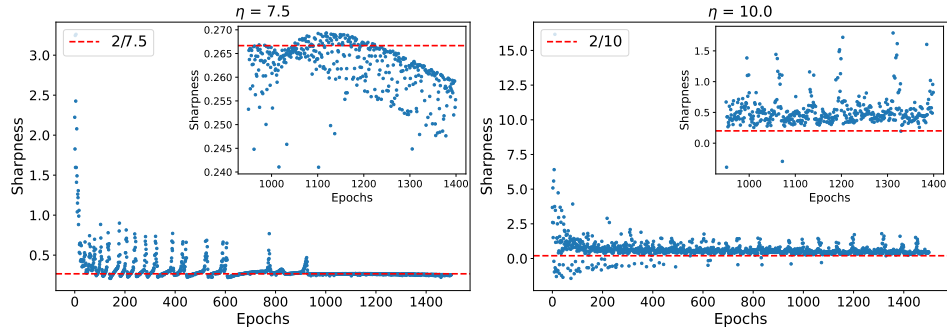


Figure S8: Evolution of sharpness as a function of training epochs. The theoretical value $2/\eta$ is indicated by the dashed red line for reference. Results are shown for learning rates values $\eta = 7.5$ and $\eta = 10$.

-
- [1] Ian J. Goodfellow, Yoshua Bengio, and Aaron Courville. *Deep Learning*. MIT Press, Cambridge, MA, USA, 2016. <http://www.deeplearningbook.org>.
- [2] Charu C Aggarwal. *Neural networks and deep learning*, volume 10. Springer, 2018.
- [3] Lucas Lacasa, Jorge P Rodriguez, and Victor M Eguiluz. Correlations of network trajectories. *Physical Review Research*, 4(4):L042008, 2022.
- [4] Luís A Nunes Amaral. Artificial intelligence needs a scientific method-driven reset. *Nature Physics*, 20(4):523–524, 2024.
- [5] Ginestra Bianconi, Alex Arenas, Jacob Biamonte, Lincoln D Carr, Byungnam Kahng, Janos Kertesz, Jürgen Kurths, Linyuan Lü, Cristina Masoller, Adilson E Motter, et al. Complex systems in the spotlight: next steps after the 2021 nobel prize in physics. *Journal of Physics: Complexity*, 4(1):010201, 2023.
- [6] Lluís Arola-Fernández and Lucas Lacasa. Effective theory of collective deep learning. *Physical Review Research*, 6(4):L042040, 2024.
- [7] Kaloyan Danovski, Miguel C Soriano, and Lucas Lacasa. Dynamical stability and chaos in artificial neural network trajectories along training. *Frontiers in Complex Systems*, 2:1367957, 2024.
- [8] Vito Latora, Vincenzo Nicosia, and Giovanni Russo. *Complex networks: principles, methods and applications*. Cambridge University Press, 2017.
- [9] Petter Holme and Jari Saramäki. Temporal networks. *Physics reports*, 519(3):97–125, 2012.
- [10] Naoki Masuda and Renaud Lambiotte. *A guide to temporal networks*. World Scientific, 2016.
- [11] Arash Badie-Modiri, Chiara Boldrini, Lorenzo Valerio, János Kertész, and Márton Karsai. Initialisation and network effects in decentralised federated learning. *arXiv preprint arXiv:2403.15855*, 2024.
- [12] Emanuele La Malfa, Gabriele La Malfa, Giuseppe Nicosia, and Vito Latora. Deep neural networks via complex network theory: a perspective. *arXiv preprint arXiv:2404.11172*, 2024.
- [13] Ziwei Zheng, Huizhi Liang, Vaclav Snašel, Vito Latora, Panos Pardalos, Giuseppe Nicosia, and Varun Ojha. On learnable parameters of optimal and suboptimal deep learning models. *arXiv preprint arXiv:2408.11720*, 2024.
- [14] Heinz Georg Schuster and Wolfram Just. *Deterministic chaos: an introduction*. John Wiley & Sons, 2006.
- [15] Holger Kantz and Thomas Schreiber. *Nonlinear time series analysis*. Cambridge university press, 2003.
- [16] Dimitri Bertsekas, Angelia Nedic, and Asuman Ozdaglar. *Convex analysis and optimization*, volume 1. Athena Scientific, 2003.
- [17] Lingkai Kong and Molei Tao. Stochasticity of deterministic gradient descent: Large learning rate for multiscale objective function. *Advances in neural information processing systems*, 33:2625–2638, 2020.
- [18] Ying-Cheng Lai and Tamás Tél. *Transient chaos: complex dynamics on finite time scales*, volume 173. Springer Science & Business Media, 2011.
- [19] Matej Črepinšek, Shih-Hsi Liu, and Marjan Mernik. Exploration and exploitation in evolutionary algorithms: A survey. *ACM computing surveys (CSUR)*, 45(3):1–33, 2013.
- [20] Oded Berger-Tal, Jonathan Nathan, Ehud Meron, and David Saltz. The exploration-exploitation dilemma: a multidisciplinary framework. *PLoS one*, 9(4):e95693, 2014.
- [21] Nicolas E Humphries, Henri Weimerskirch, Nuno Queiroz, Emily J Southall, and David W Sims. Foraging success of biological lévy flights recorded in situ. *Proceedings of the National Academy of Sciences*, 109(19):7169–7174, 2012.
- [22] Gabriel Ramos-Fernández, José L Mateos, Octavio Miramontes, Germinal Cocho, Hernán Larralde, and Barbara Ayala-Orozco. Lévy walk patterns in the foraging movements of spider monkeys (ateles geoffroyi). *Behavioral ecology and Sociobiology*, 55:223–230, 2004.
- [23] Sigrunn Eliassen, Christian Jørgensen, Marc Mangel, and Jarl Giske. Exploration or exploitation: life expectancy changes the value of learning in foraging strategies. *Oikos*, 116(3):513–523, 2007.
- [24] Andy Reynolds, Eliane Ceccon, Cristina Baldauf, Tassia Karina Medeiros, and Octavio Miramontes. Lévy foraging patterns of rural humans. *PLoS one*, 13(6):e0199099, 2018.
- [25] Jackelyn M Kembro, Mathieu Lihoreau, Joan Garriga, Ernesto P Raposo, and Frederic Bartumeus. Bumblebees learn foraging routes through exploitation–exploration cycles. *Journal of the Royal Society Interface*, 16(156):20190103, 2019.
- [26] Christopher T Monk, Matthieu Barbier, Pawel Romanczuk, James R Watson, Josep Alós, Shinnosuke Nakayama, Daniel I Rubenstein, Simon A Levin, and Robert Arlinghaus. How ecology shapes exploitation: a framework to predict the behavioural response of human and animal foragers along exploration–exploitation trade-offs. *Ecology letters*, 21(6):779–793, 2018.
- [27] Leticia R Paiva, Sidiney G Alves, Lucas Lacasa, Og DeSouza, and Octavio Miramontes. Visibility graphs of animal foraging trajectories. *Journal of Physics: Complexity*, 3(4):04LT03, 2022.
- [28] Rainer Klages, Günter Radons, and Igor Mihajlović Sokolov. *Anomalous transport*. Wiley Online Library, 2008.
- [29] Thomas T Hills, Peter M Todd, David Lazer, A David Redish, and Iain D Couzin. Exploration versus exploitation in space, mind, and society. *Trends in cognitive sciences*, 19(1):46–54, 2015.
- [30] Merideth A Addicott, John M Pearson, Maggie M Sweitzer, David L Barack, and Michael L Platt. A primer on foraging and the explore/exploit trade-off for psychiatry research. *Neuropsychopharmacology*, 42(10):1931–1939, 2017.
- [31] Shin Ishii, Wako Yoshida, and Junichiro Yoshimoto. Control of exploitation–exploration meta-parameter in reinforcement learning. *Neural networks*, 15(4-6):665–687, 2002.
- [32] Nils Bertschinger, Thomas Natschläger, and Robert Legenstein. At the edge of chaos: Real-time computations and self-organized criticality in recurrent neural networks. *Advances in neural information processing systems*, 17, 2004.

- [33] Jonathan Kadmon and Haim Sompolinsky. Transition to chaos in random neuronal networks. *Physical Review X*, 5(4):041030, 2015.
- [34] David Sussillo and Larry F Abbott. Generating coherent patterns of activity from chaotic neural networks. *Neuron*, 63(4):544–557, 2009.
- [35] Ulises Pereira-Obilinovic, Johnatan Aljadeff, and Nicolas Brunel. Forgetting leads to chaos in attractor networks. *Physical Review X*, 13(1):011009, 2023.
- [36] Diego Pazó. Discontinuous transition to chaos in a canonical random neural network. *Physical Review E*, 110(1):014201, 2024.
- [37] Jingyi Luo, Jianyu Chen, and Hong-Kun Zhang. The butterfly effect in neural networks: Unveiling hyperbolic chaos through parameter sensitivity. *Neural Networks*, page 107572, 2025.
- [38] Jeremy Cohen, Simran Kaur, Yuanzhi Li, J Zico Kolter, and Ameet Talwalkar. Gradient descent on neural networks typically occurs at the edge of stability. In *International Conference on Learning Representations*, 2021.
- [39] Chris G Langton. Computation at the edge of chaos: Phase transitions and emergent computation. *Physica D: nonlinear phenomena*, 42(1-3):12–37, 1990.
- [40] Yann LeCun. The mnist database of handwritten digits. <http://yann.lecun.com/exdb/mnist/>, 1998.
- [41] Annalisa Caligiuri, Victor M. Eguíluz, Leonardo Di Gaetano, Tobias Galla, and Lucas Lacasa. Lyapunov exponents for temporal networks. *Phys. Rev. E*, 107:044305, Apr 2023.
- [42] Ronald A Fisher. The use of multiple measurements in taxonomic problems. *Annals of eugenics*, 7(2):179–188, 1936.
- [43] Yann LeCun, Léon Bottou, Yoshua Bengio, and Patrick Haffner. Gradient-based learning applied to document recognition. *Proceedings of the IEEE*, 86(11):2278–2324, 1998.
- [44] A. Krizhevsky and G. Hinton. Learning multiple layers of features from tiny images. *Master’s thesis, Department of Computer Science, University of Toronto*, 2009.
- [45] Zhouhan Lin, Roland Memisevic, and Kishore Konda. How far can we go without convolution: Improving fully-connected networks. *arXiv preprint arXiv:1511.02580*, 2015.